



HAL
open science

Analytical buckling analysis of an inflatable beam made of orthotropic technical textiles

Thanh-Truong Nguyen, S Ronel, M Massenzio, Kl Apedo, E Jacquelin

► **To cite this version:**

Thanh-Truong Nguyen, S Ronel, M Massenzio, Kl Apedo, E Jacquelin. Analytical buckling analysis of an inflatable beam made of orthotropic technical textiles. *Thin-Walled Structures*, 2012, 51, pp.186-200. 10.1016/j.tws.2011.10.017 . hal-00951842

HAL Id: hal-00951842

<https://hal.science/hal-00951842>

Submitted on 28 May 2018

HAL is a multi-disciplinary open access archive for the deposit and dissemination of scientific research documents, whether they are published or not. The documents may come from teaching and research institutions in France or abroad, or from public or private research centers.

L'archive ouverte pluridisciplinaire **HAL**, est destinée au dépôt et à la diffusion de documents scientifiques de niveau recherche, publiés ou non, émanant des établissements d'enseignement et de recherche français ou étrangers, des laboratoires publics ou privés.

Analytical buckling analysis of an inflatable beam made of orthotropic technical textiles

Thanh-Truong Nguyen^{a,b,c,*}, S. Ronel^{a,b,c}, M. Massenzio^{a,b,c}, K.L. Apedo^{a,b,c}, E. Jacquelin^{a,b,c}

^a Université de Lyon, F-69622 Lyon, France

^b IFSTTAR, UMR_T9406, LBMC, F-69675 Bron, France

^c Université Lyon 1, Villeurbanne, France

An analytical approach was considered to study the buckling and the behavior of an inflatable orthotropic beam subjected to uniform compression loads under different boundary conditions. In order to assess the stability of inflatable structures, it is necessary to evaluate the critical load of the inflatable components in their pressurized configurations. First, a 3D inflatable orthotropic beam model based on the Timoshenko's kinematics was briefly introduced: the nonlinearities (finite rotation, follower forces) were included in this model. The nonlinear equilibrium equations were derived from the total Lagrangian form of the virtual work principle: the linearized equations were then obtained. By solving these linearized equations, an analytical expression of the critical buckling load was obtained. This critical buckling load was investigated through several load cases with several boundary conditions. The discrepancy due to the orthotropic character between the present model and the isotropic models found in the literature was evaluated, as well as the influence of the inflation pressure and the fabric mechanical properties on the value of critical load. The buckling mode shapes were also determined. To check the limit of validity of the results, the wrinkling load was also presented in every case.

1. Introduction

The homogeneous orthotropic woven fabrics (HOWF) were formerly developed as substrates for flexible coated textiles. They play an important role in many industrial applications due to their outstanding mechanical properties. At the beginning of the 1990s, the HOWF entered the field of the rigid structural composites and have produced a variety of space and terrestrial structures. This is a consequence of their outstanding physical, thermal, and mechanical properties (particularly lightweight), high stiffness and strength. Such applications require a good knowledge of the material to design, and to optimize the structures.

A large number of analytical analyses related to the inflatable beams and arches have been already published. These studies concerned both theoretical and experimental analysis. One important aspect is the need to build the best adapted analytical model for these structures. In order to derive the analytical solutions and to develop the formulations for inflatable beams made from woven fabrics, two beam kinematics assumptions have been used: the Euler Bernoulli kinematics and the Timoshenko kinematics.

Most earlier researches have been based on the Euler Bernoulli kinematics. Thus, Comer and Levy [1] have derived a load deflection theory in the case of an isotropic material where the beam material has been supposed to be tension-only linear elastic. Afterward, Main et al. [2] have developed a method for analyzing the inflated fabric beams with a model analogous to the shear-moment method; their work was based on Comer and Levy's theory that had been modified to reflect the wrinkling behavior of the fabric. In a second paper [3], they improved their theory with an orthotropic membrane model.

Meanwhile, Fichter [4] developed a theory for a homogeneous isotropic fabric inflated beam based on the Timoshenko kinematics. His study has shown that the Timoshenko kinematics is more suitable for this kind of structure. His linearized equations have pointed out that the internal pressure increases the shear stiffness of the beam-column. In order to improve Fichter's theory, Le van and Wielgosz [5] proposed a new formulation for the inflatable beams with the Timoshenko kinematics by considering the finite rotations. Davids and Zhang [6] focused on the development of a Timoshenko beam finite element for the nonlinear load-deflection analysis of pressurized fabric beams. They addressed numerically the pressure effect on the beam behavior.

Nevertheless, the previous studies have only been investigated on 2D linearized inflatable beams. Also, the fabric was often supposed to be hyperelastic isotropic and the Saint Venant-Kirchhoff hypothesis was always used as for the traditional beams. More recently, Apedo et al. [7] performed a theoretical analysis of

* Corresponding author at: Université de Lyon, F-69622 Lyon, France.

Tel.: +33 4 72 65 64; fax: +33 4 72 65 53 54.

E-mail addresses: thtruong@gmail.com,

truong.nguyen-thanh@etu.univ-lyon1.fr (T.-T. Nguyen).

inflatable beams in which a homogeneous orthotropic fabric was considered. A 3D Timoshenko beam model has been developed, and, by using the total Lagrangian form of the virtual work principle, the nonlinear equations have been obtained: as an example, the bending problem has been investigated [7,8].

Buckling and wrinkling, the important design considerations for inflatable beam-columns or arches, have not been very much investigated. Fichter [4] used the minimization of the global potential energy to calculate the buckling load of an inflated column. Fichter's equations for the buckling load have shown that the internal pressure increases the resistance to the transverse shear deformation and have shown that the buckling loads are lower than those predicted using Euler's buckling theory. Further works conducted by Le van and Wielgosz [5,9] have provided a good approximation for the critical load for a cantilever beam. Their results have shown that the buckling load is not only a function of the mechanical properties but also of the inflation pressure. The increase of one of these parameters leads to an increase of the buckling load.

In this paper, an analytical approach for the buckling problem is performed using the linearized equations derived in Apedo et al. [7]. The analytical solution of the critical buckling load is investigated for various boundary conditions. A parametric study is carried out in order to assess the influence of the inflation pressure and the fabric mechanical properties on the critical load. Finally, the limit of validity of the results is addressed.

2. Theoretical background

In this section the governing equations of a 3D Timoshenko beam with a HOWF are briefly presented. The Green–Lagrange strain measure is used due to the geometrical nonlinearities.

Fig. 1 shows an inflatable cylindrical beam made of an HOWF. l_0 , R_0 , t_0 , A_0 and I_0 represent respectively the length, the fabric thickness, the external radius, the cross-section and the moment of inertia around the principal axes of inertia Y and Z of the beam in the reference configuration which is the inflated configuration. A_0 and I_0 are given by

$$A_0 = 2\pi R_0 t_0 \quad (1)$$

$$I_0 = \frac{A_0 R_0^2}{2} \quad (2)$$

where the reference dimensions l_0 , R_0 and t_0 depend on the inflation pressure and the mechanical properties of the fabric [7]:

$$l_0 = l_\phi + \frac{pR_\phi l_\phi}{2E_t t_\phi} (1 - 2\nu_{lt}) \quad (3a)$$

$$R_0 = R_\phi + \frac{pR_\phi^2}{2E_t t_\phi} (2 - \nu_{lt}) \quad (3b)$$

$$t_0 = t_\phi - \frac{3pR_\phi}{2E_t} \nu_{lt} \quad (3c)$$

in which l_ϕ , R_ϕ , and t_ϕ are respectively the length, the fabric thickness, and the external radius of the beam in the natural state.

The internal pressure p is assumed to remain constant, which simplifies the analysis and is consistent with the experimental observations and the prior studies on inflated fabric beams and arches [1–6,9–13]. The initial pressurization takes place prior to the application of concentrated and distributed external loads, and is not included in the structural analysis per se.

The slenderness ratio is $\lambda = L/\rho$ where $L = \mu l_0$ is the beam length and $\rho = \sqrt{I_0/A_0}$ is the beam radius of gyration. The coefficient μ takes different values according to the boundary conditions of the beam.

M is a point on the current cross-section and G_0 the centroid of the current cross-section lies on the X -axis. The beam is undergoing axial loading. Two Fichter's simplifying assumptions are applied in the following:

- the cross-section of the inflated beam under consideration is assumed to be circular and maintains its shape after deformation, so that there are no distortion and local buckling;
- the rotations around the principal inertia axes of the beam are small and the rotation around the beam axis is negligible.

Due to the first assumption, the model considers that no wrinkling occurs so that the ovalization problem is not addressed in this paper as done in many previous papers [4,5].

2.1. Kinematics

The material is assumed orthotropic and the warp direction of the fabric is assumed to coincide with the beam axis; thus the weft yarn is circumferential. The model can be adapted to the case where the axes are in other directions. In this case, an additional rotation may be operated to relate the orthotropic directions and the beam axes. This general case is not addressed here because, for an industrial purpose, the orthotropic principal directions coincide with the longitudinal and circumferential directions of the cylinder [14].

The displacement components of an arbitrary point $M(X,Y,Z)$ on the beam are [15,16]

$$\underline{\mathbf{u}}(M) = \begin{Bmatrix} u_x \\ u_y \\ u_z \end{Bmatrix} = \begin{Bmatrix} u(X) \\ 0 \\ 0 \end{Bmatrix} + \begin{Bmatrix} Z\theta_Y(X) \\ 0 \\ w(X) \end{Bmatrix} + \begin{Bmatrix} -Y\theta_Z(X) \\ v(X) \\ 0 \end{Bmatrix} \quad (4)$$

where u_x , u_y and u_z are the components of the displacement at the arbitrary point M , whilst $u(X)$, $v(X)$ and $w(X)$ correspond to the displacements of the centroid G_0 of the current cross-section at abscissa X , related to the base (X,Y,Z) ; $\theta_Y(X)$ and $\theta_Z(X)$ are the rotations of the current section at abscissa X around both principal axes of inertia of the beam, respectively. Let $\delta\underline{\mathbf{u}}$ denote an arbitrary virtual displacement from the current position of the

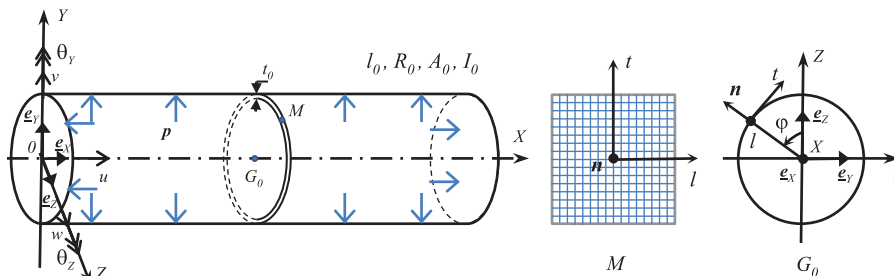


Fig. 1. HOWF inflatable beam.

material point M :

$$\delta \underline{\mathbf{u}} = \begin{Bmatrix} \delta u(X) \\ 0 \\ 0 \end{Bmatrix} + \begin{Bmatrix} Z\delta\theta_Y(X) \\ 0 \\ \delta w(X) \end{Bmatrix} + \begin{Bmatrix} -Y\delta\theta_Z(X) \\ \delta v(X) \\ 0 \end{Bmatrix} \quad (5)$$

The definition of the strain at an arbitrary point as a function of the displacements is

$$\underline{\underline{\mathbf{E}}} = \underline{\underline{\mathbf{E}}}_l + \underline{\underline{\mathbf{E}}}_{nl} \quad (6)$$

where $\underline{\underline{\mathbf{E}}}_l$ and $\underline{\underline{\mathbf{E}}}_{nl}$ are the Green–Lagrange linear and nonlinear strains, respectively. The nonlinear term $\underline{\underline{\mathbf{E}}}_{nl}$ takes into account the geometrical nonlinearities. The strain fields depend on the displacement fields as follows:

$$\underline{\underline{\mathbf{E}}}_l = \begin{Bmatrix} \frac{\partial u_x}{\partial X} \\ \frac{\partial u_y}{\partial Y} \\ \frac{\partial u_z}{\partial Z} \\ \frac{\partial u_x}{\partial Y} + \frac{\partial u_y}{\partial X} \\ \frac{\partial u_x}{\partial Z} + \frac{\partial u_z}{\partial X} \\ \frac{\partial u_y}{\partial Z} + \frac{\partial u_z}{\partial Y} \end{Bmatrix}, \quad \underline{\underline{\mathbf{E}}}_{nl} = \begin{Bmatrix} \frac{1}{2} \underline{\mathbf{u}}_X^T \underline{\mathbf{u}}_X \\ \frac{1}{2} \underline{\mathbf{u}}_Y^T \underline{\mathbf{u}}_Y \\ \frac{1}{2} \underline{\mathbf{u}}_Z^T \underline{\mathbf{u}}_Z \\ \frac{1}{2} \underline{\mathbf{u}}_X^T \underline{\mathbf{u}}_Y + \frac{1}{2} \underline{\mathbf{u}}_Y^T \underline{\mathbf{u}}_X \\ \frac{1}{2} \underline{\mathbf{u}}_X^T \underline{\mathbf{u}}_Z + \frac{1}{2} \underline{\mathbf{u}}_Z^T \underline{\mathbf{u}}_X \\ \frac{1}{2} \underline{\mathbf{u}}_Y^T \underline{\mathbf{u}}_Z + \frac{1}{2} \underline{\mathbf{u}}_Z^T \underline{\mathbf{u}}_Y \end{Bmatrix} \quad (7)$$

The higher-order nonlinear terms are the product of the vectors that are defined as

$$\underline{\mathbf{u}}_X = \begin{Bmatrix} u_{X,X} \\ u_{Y,X} \\ u_{Z,X} \end{Bmatrix}, \quad \underline{\mathbf{u}}_Y = \begin{Bmatrix} u_{X,Y} \\ u_{Y,Y} \\ u_{Z,Y} \end{Bmatrix}, \quad \underline{\mathbf{u}}_Z = \begin{Bmatrix} u_{X,Z} \\ u_{Y,Z} \\ u_{Z,Z} \end{Bmatrix} \quad (8)$$

2.2. Constitutive equations

In the present work, the Saint Venant–Kirchhoff orthotropic material is used. The energy function $\Phi_E = \Phi(\underline{\underline{\mathbf{E}}})$ in this case is also known as the Helmholtz free-energy function. The components of the second Piola–Kirchhoff tensor $\underline{\underline{\mathbf{S}}}$ are given by the nonlinear Hookean stress-strain relationships

$$\underline{\underline{\mathbf{S}}} = \underline{\underline{\mathbf{S}}}^0 + \frac{\partial \Phi}{\partial \underline{\underline{\mathbf{E}}}} = \underline{\underline{\mathbf{S}}}^0 + \underline{\underline{\mathbf{C}}} \cdot \underline{\underline{\mathbf{E}}} \quad (9)$$

where

- $\underline{\underline{\mathbf{S}}}^0$ is the inflation pressure prestressing tensor.
- the second Piola–Kirchhoff tensor is written in the beam coordinate system as

$$\underline{\underline{\mathbf{S}}} = \begin{bmatrix} S_{XX} & S_{XY} & S_{XZ} \\ & S_{YY} & S_{YZ} \\ \text{symmetrical} & & S_{ZZ} \end{bmatrix} \quad (10)$$

- $\underline{\underline{\mathbf{C}}}$ is the elasticity tensor expressed in the beam axes.

In general, the inflation pressure prestressing tensor is assumed spheric and isotropic [5]. So,

$$\underline{\underline{\mathbf{S}}}^0 = S^0 \underline{\underline{\mathbf{I}}} \quad (11)$$

where $\underline{\underline{\mathbf{I}}}$ is the identity second order tensor and $S^0 = N_0/A_0$ is the prestressing scalar. The elasticity tensor in the beam axes was transformed from the orthotropic l,t basis (see [7])

$$\underline{\underline{\mathbf{C}}} = \begin{bmatrix} C_{11} & c^2 C_{12} & s^2 C_{12} & cs C_{12} & 0 & 0 \\ & c^4 C_{22} & c^2 s^2 C_{22} & c^3 s C_{22} & 0 & 0 \\ & & s^4 C_{22} & cs^3 C_{22} & 0 & 0 \\ & & & c^2 s^2 C_{22} & 0 & 0 \\ & & & & s^2 C_{66} & cs C_{66} \\ \text{symmetrical} & & & & & c^2 C_{66} \end{bmatrix} \quad (12)$$

where $c = \cos \varphi$ and $s = \sin \varphi$ with $\varphi = (e_z, n)$ the angle between the Z -axis of the beam and the normal of the membrane at the current point. The tensor components are described as a function of the mechanical properties of the HOW fabric:

$$C_{11} = E_l / (1 - \nu_{lt} \nu_{tl}), \quad C_{12} = E_l \nu_{tl} / (1 - \nu_{lt} \nu_{tl})$$

$$C_{22} = E_t / (1 - \nu_{lt} \nu_{tl}), \quad C_{66} = G_{lt} \quad \text{and} \quad E_l / \nu_{lt} = E_t / \nu_{tl}$$

2.3. Virtual work principle

The balance equations of an inflatable beam come from the virtual work principle (VWP). The VWP applied to the beam in its pressurized state is

$$\delta W_{int} = \delta W_{ext}^d + \delta W_{ext}^p, \quad \forall \delta \underline{\mathbf{u}} \quad (13)$$

$$\Leftrightarrow \int_{V_0} \underline{\underline{\mathbf{S}}} : \delta \underline{\underline{\mathbf{E}}} dV_0 = \int_{V_0} \underline{\mathbf{f}} \cdot \delta \underline{\mathbf{u}} dV_0 + \{\underline{\mathbf{R}} \cdot \delta \underline{\mathbf{u}}\} + \int_{\partial V_0} \underline{\mathbf{t}} \cdot \delta \underline{\mathbf{u}} dA, \quad \forall \delta \underline{\mathbf{u}} \quad (14)$$

where $\underline{\mathbf{f}}$ and $\underline{\mathbf{t}}$ are the body forces per unit volume and the traction forces per unit area, respectively; $\underline{\mathbf{R}}$ represents the reactions. The internal virtual work δW_{int} on the left-hand-side of (13) is formulated from the second Piola–Kirchhoff tensor $\underline{\underline{\mathbf{S}}}$ and the virtual Green strain $\delta \underline{\underline{\mathbf{E}}}$.

The virtual Green strain tensor is written in the beam coordinate system as

$$\delta \underline{\underline{\mathbf{E}}} = \delta \underline{\underline{\mathbf{E}}}_l + \delta \underline{\underline{\mathbf{E}}}_{nl} \quad (15)$$

where

$$\delta \underline{\underline{\mathbf{E}}}_l = [\delta E_{XX}^l \quad \delta E_{YY}^l \quad \delta E_{ZZ}^l \quad \delta E_{YZ}^l \quad \delta E_{ZX}^l \quad \delta E_{XY}^l]^T \quad (16a)$$

$$\delta \underline{\underline{\mathbf{E}}}_{nl} = [\delta E_{XX}^{nl} \quad \delta E_{YY}^{nl} \quad \delta E_{ZZ}^{nl} \quad \delta E_{YZ}^{nl} \quad \delta E_{ZX}^{nl} \quad \delta E_{XY}^{nl}]^T \quad (16b)$$

with

$$\delta E_{XX}^l = \delta u_{,X} + Z\delta\theta_{Y,X} - Y\delta\theta_{Z,X}$$

$$\delta E_{YY}^l = 0$$

$$\delta E_{ZZ}^l = 0$$

$$\delta E_{YZ}^l = 0$$

$$\delta E_{XZ}^l = \delta w_{,X} + \delta\theta_{Y,X}$$

$$\delta E_{XY}^l = \delta v_{,X} - \delta\theta_Z \quad (17)$$

and

$$\begin{aligned} \delta E_{XX}^{nl} &= (u_{,X} + Z\theta_{Y,X} - Y\theta_{Z,X})\delta u_{,X} + v_{,X}\delta v_{,X} \\ &\quad + w_{,X}\delta w_{,X} + Z(u_{,X} + Z\theta_{Y,X} - Y\theta_{Z,X})\delta\theta_{Y,X} \\ &\quad - Y(u_{,X} + Z\theta_{Y,X} - Y\theta_{Z,X})\delta\theta_{Z,X} \end{aligned}$$

$$\delta E_{YY}^{nl} = \theta_Z \delta\theta_Z$$

$$\delta E_{ZZ}^{nl} = \theta_Y \delta\theta_Y$$

$$\delta E_{YZ}^{nl} = (\theta_Z \delta\theta_Y + \theta_Y \delta\theta_Z)$$

$$\delta E_{XZ}^{nl} = \theta_Y \delta u_{,X} + (u_{,X} + Z\theta_{Y,X} - Y\theta_{Z,X})\delta\theta_Y + Z\theta_Y \delta\theta_{Y,X} - Y\theta_Y \delta\theta_{Z,X}$$

$$\delta E_{XY}^{nl} = -\theta_Z \delta u_{,X} - Z\theta_Z \delta\theta_{Y,X} - s(u_{,X} + Z\theta_{Y,X} - Y\theta_{Z,X})\delta\theta_Z + Y\theta_Z \delta\theta_{Z,X} \quad (18)$$

The generalized resultant forces and moments, and the quantities Q_i ($i = 1, \dots, 10$) acting over the reference cross-section A_0 can be

related to the stresses in the beam by

$$\begin{Bmatrix} N \\ T_y \\ T_z \\ M_y \\ M_z \end{Bmatrix} = \int_{A_0} \begin{Bmatrix} S_{XX} \\ S_{XY} \\ S_{XZ} \\ ZS_{XX} \\ -YS_{XX} \end{Bmatrix} dA_0 \quad (19)$$

$$Q_i = \int_{A_0} \begin{Bmatrix} -YZS_{XX} \\ Z^2S_{XX} \\ -ZS_{XY} \\ ZS_{XZ} \\ Y^2S_{XX} \\ YS_{XY} \\ -YS_{XZ} \\ S_{YY} \\ S_{ZZ} \\ -S_{YZ} \end{Bmatrix} dA_0, \quad i = 1, \dots, 10 \quad (20)$$

where N corresponds to the axial force, T_y and T_z to the shear force in Y and Z directions respectively, M_y and M_z to the bending moments about the Y - and Z -axes. Quantities Q_i depend on the initial geometry of the cross-section and are given in the Appendix. Then the internal virtual work may be written as

$$-\delta W_{int} = \int_0^{l_0} \begin{Bmatrix} A_1(X) \\ B_1(X) \\ C_1(X) \\ D_1(X) \\ E_1(X) \\ F_1(X) \\ H_1(X) \end{Bmatrix}^T \times \begin{Bmatrix} \delta u_{,x} \\ \delta v_{,x} \\ \delta w_{,x} \\ \delta \theta_Y \\ \delta \theta_{Y,x} \\ \delta \theta_Z \\ \delta \theta_{Z,x} \end{Bmatrix} dX \quad (21)$$

With the terms $A_1(X)$, $B_1(X)$, $C_1(X)$, $D_1(X)$, $E_1(X)$, $F_1(X)$ and $H_1(X)$ are given in the Appendix.

The external virtual work δW_{ext} is due to the dead loads and to the pressure load. The dead loads, which may include concentrated loads and moments as well as distributed loads, act like the body forces. The inflation pressure plays a role of a traction force acting on the cylindrical surface and on both ends. The first term on the right side of (14) can be rewritten as

$$\delta W_{ext}^d = \int_0^{l_0} \begin{Bmatrix} f_x \\ f_y \\ f_z \end{Bmatrix}^T \times \begin{Bmatrix} \delta u \\ \delta v \\ \delta w \end{Bmatrix} dX + \sum_{i=1}^n \begin{Bmatrix} F_X(X_i) \\ F_Y(X_i) \\ F_Z(X_i) \\ M_Y(X_i) \\ M_Z(X_i) \end{Bmatrix}^T \times \begin{Bmatrix} \delta u(X_i) \\ \delta v(X_i) \\ \delta w(X_i) \\ \delta \theta_Y(X_i) \\ \delta \theta_Z(X_i) \end{Bmatrix} \quad (22)$$

In which f_x , f_y and f_z are respectively the distributed loads along the X -, Y -, and Z -axes, while $F_a(b)$, and $M_a(b)$ (with $a = X, Y, Z; b = X_1, \dots, X_n$) are the external support reactions and the external loads and moments.

The second term on the right side of (14) is the external virtual work due to the inflation pressure. This virtual work includes the pressure virtual work on the cylindrical surface δW_{cyl}^p and on both ends δW_{end}^p . Fig. 2 shows a reference cylindrical inflated beam with an applied uniform pressure p acting on the cylindrical surface A which has a pointwise normal \mathbf{n} in the current configuration. The traction force vector \mathbf{t} in (14) is therefore $p\mathbf{n}$ and the

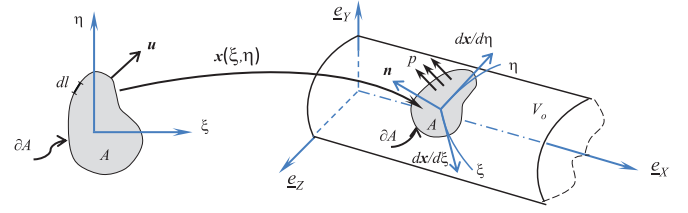


Fig. 2. Uniform pressure on the cylindrical surface.

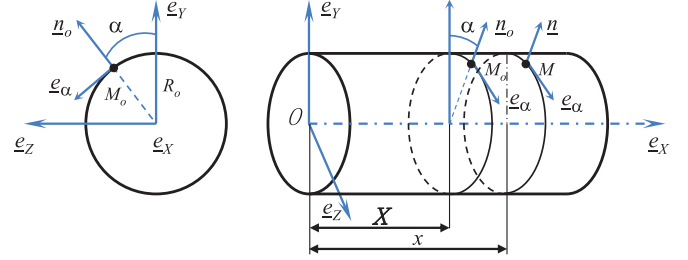


Fig. 3. Definition of the curvilinear coordinate system.

virtual work due to the inflation pressure δW_{ext}^p is then given by

$$\delta W_{ext}^p = \delta W_{cyl}^p + \delta W_{end}^p = \int_A p \mathbf{n} \cdot \delta \mathbf{u} dA \quad (23)$$

To determine the pressure virtual work δW_{cyl}^p , the curvilinear coordinates (ξ, η) are used (Fig. 3):

$$\begin{cases} \xi = R_0 \alpha \\ \eta = X \end{cases} \quad (24)$$

where α is the polar angle between the normal \mathbf{n} at a current position \underline{x} and the \underline{e}_Y . The coordinates of a material point M_0 are given by

$$\underline{OM}_0 = \underline{X} = \begin{cases} X \\ R_0 \cos \alpha \\ R_0 \sin \alpha \end{cases} \quad (25)$$

The position vector at the current configuration is then given by

$$\underline{OM} = \underline{x} = \underline{X} + \underline{U} = \begin{cases} X + u(X) - R_0 \theta_Z \cos \alpha + R_0 \theta_Y \sin \alpha \\ v(X) + R_0 \cos \alpha \\ w(X) + R_0 \sin \alpha \end{cases} \quad (26)$$

By using an arbitrary parameterization of the surface as shown in Fig. 2, the normal and area elements can be obtained in terms of the tangent vectors $\partial \underline{x} / \partial \xi$ and $\partial \underline{x} / \partial \eta$ as

$$\mathbf{n} = \frac{\frac{\partial \underline{x}}{\partial \xi} \times \frac{\partial \underline{x}}{\partial \eta}}{\left\| \frac{\partial \underline{x}}{\partial \xi} \times \frac{\partial \underline{x}}{\partial \eta} \right\|} = \frac{\frac{\partial \underline{x}}{R_0 \partial \alpha} \times \frac{\partial \underline{x}}{\partial X}}{\left\| \frac{\partial \underline{x}}{R_0 \partial \alpha} \times \frac{\partial \underline{x}}{\partial X} \right\|} \quad (27)$$

and

$$dA = \left\| \frac{\partial \underline{x}}{\partial \xi} \times \frac{\partial \underline{x}}{\partial \eta} \right\| d\xi d\eta = \left\| \frac{\partial \underline{x}}{R_0 \partial \alpha} \times \frac{\partial \underline{x}}{\partial X} \right\| R_0 d\alpha dX. \quad (28)$$

Then δW_{cyl}^p is

$$\delta W_{cyl}^p = \int_A p \cdot \delta \mathbf{u} \cdot \left(\frac{\partial \underline{x}}{\partial \xi} \times \frac{\partial \underline{x}}{\partial \eta} \right) d\xi d\eta \quad (29)$$

$$\delta W_{cyl}^p = F_p \int_0^{l_0} [-\theta_{Z,x} \quad \theta_{Y,x} \quad -w_{,x} \quad v_{,x}] \times \begin{Bmatrix} \delta v \\ \delta w \\ \delta \theta_Y \\ \delta \theta_Z \end{Bmatrix} dX \quad (30)$$

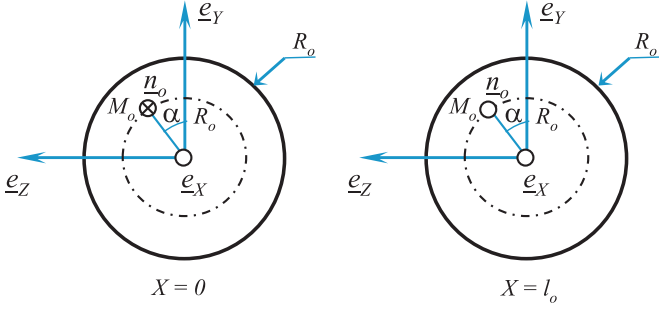


Fig. 4. Definition of the curvilinear basis at the beam ends.

The pressure virtual work at the ends of the beam can be determined in the same way: the reference circular end surfaces ($X=0$ and $X=l_0$) can be represented by the curvilinear coordinates $(\xi, \eta) = (r, r\alpha)$ (Fig. 4). Then,

$$\delta W_{end}^p = \int_A \underline{p} \cdot \delta \underline{u}(l_0) dA - \int_A \underline{p} \cdot \delta \underline{u}(0) dA \quad (31)$$

$$\delta W_{end}^p = \left[\begin{matrix} 1 & \theta_Z(X_0) & -\theta_Y(X_0) \end{matrix} \right] \times \left\{ \begin{matrix} \delta u(X_0) \\ \delta v(X_0) \\ \delta w(X_0) \end{matrix} \right\} \Big|_0^{l_0} \quad (32)$$

Finally, from (29) and (31) δW_{ext}^p is given by

$$\delta W_{ext}^p = F_p \int_0^{l_0} \left[-\theta_{Z,X} \quad \theta_{Y,X} \quad -w_{,X} \quad v_{,X} \right] \times \left\{ \begin{matrix} \delta v \\ \delta w \\ \delta \theta_Y \\ \delta \theta_Z \end{matrix} \right\} dX + \left[\begin{matrix} 1 & \theta_Z(X_0) & -\theta_Y(X_0) \end{matrix} \right] \times \left\{ \begin{matrix} \delta u(X_0) \\ \delta v(X_0) \\ \delta w(X_0) \end{matrix} \right\} \Big|_0^{l_0} \quad (33)$$

where $F_p = pIR_0^2$ is the pressure force due to the inflation pressure.

One can note that, according to (33), the follower force effect of the external load due to the inflation pressure depends on the displacements and the rotations.

2.4. Theoretical buckling loads

To obtain an analytical solution for the buckling loads of an inflatable orthotropic fabric beam, a linearization of the equilibrium equations derived from the VWP (13) is performed around the prestressed reference configuration of the beam assuming that the service load does not cause a large variation of the displacements obtained after the inflation [4,5]. Previous works have applied the approach to inflatable beams made from an isotropic fabric and under in-plane loading. These studies have proven that the linearized equations are well adapted to the highly inflated isotropic beams. The usual assumptions on the displacement and the rotation magnitudes let to consider that $u/l_0, v/l_0, w/l_0, \theta_Y, \theta_Z$ are small with respect to 1 [17]. In the case of buckling, the problem has only an axial concentrated load: $f_x = f_y = f_z = 0$. The linearization of the equilibrium equations (13) leads to the following equations [7]:

$$(N^0 + C_{11}A_0)u^{(2)}(X) = 0 \quad (34a)$$

$$(N^0 + \frac{1}{2}k_y A_0 C_{66})v^{(2)}(X) - (F_p + \frac{1}{2}k_y A_0 C_{66})\theta_Z^{(1)}(X) = 0 \quad (34b)$$

$$(N^0 + \frac{1}{2}k_z A_0 C_{66})w^{(2)}(X) + (F_p + \frac{1}{2}k_z A_0 C_{66})\theta_Y^{(1)}(X) = 0 \quad (34c)$$

$$C_{11} + \frac{N^0}{A_0} I_0 \theta_Y^{(2)}(X) - \left(F_p + \frac{1}{2}k_z A_0 C_{66} \right) w^{(1)}(X) - \left(N^0 + \frac{1}{2}k_z A_0 C_{66} \right) \theta_Y(X) = 0 \quad (34d)$$

$$C_{11} + \frac{N^0}{A_0} I_0 \theta_Z^{(2)}(X) + \left(F_p + \frac{1}{2}k_y A_0 C_{66} \right) v^{(1)}(X) - \left(N^0 + \frac{1}{2}k_y A_0 C_{66} \right) \theta_Z(X) = 0 \quad (34e)$$

At $X=0$ and $X=l_0$, the linearized boundary conditions can be expressed as

$$N^0 + (N^0 + C_{11}A_0)u^{(1)}(X) + F_X(X) - F_p = 0 \quad (35a)$$

$$(N^0 + \frac{1}{2}k_y A_0 C_{66})v^{(1)}(X) - (F_p + \frac{1}{2}k_y A_0 C_{66})\theta_Z(X) + F_Y(X) = 0 \quad (35b)$$

$$(N^0 + \frac{1}{2}k_z A_0 C_{66})w^{(1)}(X) + (F_p + \frac{1}{2}k_z A_0 C_{66})\theta_Y(X) + F_Z(X) = 0 \quad (35c)$$

$$C_{11} + \frac{N^0}{A_0} I_0 \theta_Y^{(1)}(X) + M_Y(X) = 0 \quad (35d)$$

$$C_{11} + \frac{N^0}{A_0} I_0 \theta_Z^{(1)}(X) + M_Z(X) = 0 \quad (35e)$$

in which, the so-called correction shear coefficients k_y and k_z are determined from the shape of the cross-section. The value usually found in the literature [18] for circular thin tubes is $k_y = k_z = 0.5$. The equilibrium equations are uncoupled by the linearization process. Hence, one makes the resolution only in the in-plane loading case. By differentiating two times Eq. (34b) and one time Eq. (34e), and by substituting $\theta_Z^{(2)}(X)$ and $\theta_Z^{(1)}(X)$, one obtains the differential equation in $v(X)$:

$$v^{(4)}(X) + \frac{(F_p + N^0 + C_s^0)(F_p - N^0)}{\left(C_{11} + \frac{N^0}{A_0} \right) I_0 (N^0 + C_s^0)} v^{(2)}(X) = 0 \quad (36)$$

where $C_s^0 = \frac{1}{2}k_y A_0 C_{66}$, and $(F_p + C_s^0)$ is the shear stiffness of the inflatable beam in the case of an orthotropic fabric.

By doing the same operations on Eqs. (34b) and (34e) and now by substituting $v^{(4)}(X)$ and $v^{(2)}(X)$, one obtains the differential equation in $\theta_Z(X)$:

$$\theta_Z^{(3)}(X) + \frac{(F_p + N^0 + 2C_s^0)(F_p - N^0)}{\left(C_{11} + \frac{N^0}{A_0} \right) I_0 (N^0 + C_s^0)} \theta_Z^{(1)}(X) = 0 \quad (37)$$

From the equilibrium (34a) together with the boundary conditions (35a), the initial force $N^0(X) = F_p - F$ is derived. Relations (36) and (37) in this case become

$$v^{(4)}(X) + \frac{(2F_p - F + 2C_s^0)F}{\left(C_{11} + \frac{F_p - F}{A_0} \right) I_0 (F_p - F + C_s^0)} v^{(2)}(X) = 0 \quad (38a)$$

$$\theta_Z^{(3)}(X) + \frac{(2F_p - F + 2C_s^0)F}{\left(C_{11} + \frac{F_p - F}{A_0} \right) I_0 (F_p - F + C_s^0)} \theta_Z^{(1)}(X) = 0 \quad (38b)$$

These equations can be rewritten as

$$\begin{cases} v^{(4)}(X) + \Omega^2 v^{(2)}(X) = 0 \\ \theta_Z^{(3)}(X) + \Omega^2 \theta_Z^{(1)}(X) = 0 \end{cases} \quad (39)$$

where

$$\Omega^2 = \frac{(2F_p - F + 2C_s^0)F}{\left(C_{11} + \frac{F_p - F}{A_0}\right)I_0(F_p - F + C_s^0)} \quad (40)$$

Ω is a coefficient dependent on the fabric properties and the applied force.

The coefficient Ω is related to the buckling configurations and can be obtained from the general solution of the differential equations together with the boundary conditions. The general solution of (39) is [19]

$$\begin{cases} v(X) = B_1 \sin(\Omega X) + B_2 \cos(\Omega X) + B_3 \left(\frac{X}{I_0}\right) + B_4 \\ \theta_z(X) = C_1 \sin(\Omega X) + C_2 \cos(\Omega X) + C_3 \end{cases} \quad (41)$$

Note that the arbitrary constants of integration $B_1, B_2, B_3, B_4, C_1, C_2$ and C_3 are connected through relations (34a) and (34e). The general solution (41) then becomes

$$\begin{cases} v(X) = B_1 \sin(\Omega X) + B_2 \cos(\Omega X) + B_3 \frac{X}{I_0} + B_4 \\ \theta_z(X) = -B_2 \Omega \Gamma \sin(\Omega X) + B_1 \Omega \Gamma \cos(\Omega X) + \frac{B_3}{I_0 \Gamma} \end{cases} \quad (42)$$

The application of the method is illustrated in Section 3 with different boundary conditions.

From (40), one obtains the equation, from which the critical loads and their corresponding shapes can be evaluated. This equation is quadratic in terms of F as

$$\begin{aligned} 1 + \frac{I_0 \Omega^2}{A_0} F^2 - \left[\left(C_{11} + \frac{F_p}{A_0} \right) I_0 \Omega^2 + 2 + \frac{I_0 \Omega^2}{A_0} \right] (F_p + C_s^0) F \\ + \left(C_{11} + \frac{F_p}{A_0} \right) I_0 \Omega^2 (F_p + C_s^0) = 0 \end{aligned} \quad (43)$$

The critical load F_c is determined as the smallest root of (43). The coefficients of this quadratic equation are denoted A, B, C :

$$\begin{aligned} A &= 1 + \frac{I_0 \Omega^2}{A_0} \\ B &= - \left[\left(C_{11} + \frac{F_p}{A_0} \right) I_0 \Omega^2 + 2 + \frac{I_0 \Omega^2}{A_0} \right] (F_p + C_s^0) \\ C &= \left(C_{11} + \frac{F_p}{A_0} \right) I_0 \Omega^2 (F_p + C_s^0) \end{aligned} \quad (44)$$

Eq. (43) has two positive solutions F_{c1} and F_{c2} . The critical load is then

$$F_{cr} = \min(F_{c1}, F_{c2}) = \frac{-B - \sqrt{B^2 - 4AC}}{2A} \quad (45)$$

This relation is the main result of this paper.

2.5. Previous works on the critical load

Fichter [4] obtained the expression for the critical load of the inflated circular membranes with Timoshenko's kinematics and by using the Saint Venant–Kirchhoff hypothesis:

$$F_{cr}^{Fichter} = \frac{E^* \Gamma^* \Omega^2 (F_p + C_s^f)}{E^* \Gamma^* \Omega^2 + F_p + C_s^f} \quad (46)$$

where, $E^* = Et_0$, $G^* = Gt_0$, $A^* = A_0/t_0$, $I^* = I_0/t_0$, are respectively the membrane elastic modulus, the membrane shear modulus, the ratio of the cross-section area, and the ratio of the moment of inertia of the beam by its reference thickness t_0 . The bending stiffness and the shear stiffness coefficient are $E^* \Gamma^* \Omega^2$ and $C_s^f = G^* \pi R t_0$, respectively. The shear stiffness of the inflated beam $(F_p + C_s^f)$ included the shear stiffness provided by the internal pressure.

Le van and Wielgosz [5] (isotropic beam and Timoshenko's kinematics) obtained the following critical load:

$$F_{cr}^{Wielgosz} = \frac{\left(E + \frac{F_p}{A_0}\right) I_0 \Omega^2}{1 + \Omega^2 \frac{I_0}{A_0} + \Omega^2 \frac{\left(E + \frac{F_p I_0}{A_0}\right)}{F_p + C_s^w}} \quad (47)$$

where E is the Young modulus of the isotropic fabric and the shear stiffness coefficient $C_s^w = kGA_0$ (with $k=0.5$, a correction of the shear coefficient determined from the shape of the cross-section [18]). To entail formula (47), Le van and Wielgosz neglected the quadratic term in their equation of the critical load due to the very small radius of gyration of the beams used in their work.

Together with the boundary condition (35b) and (35e), the value of the critical load and the buckling modes in three cases are studied in the next section.

3. Examples: in-plane buckling for linearized problems

In this section, the buckling of an inflatable beam with various boundary conditions is treated. The analytical expression (45) of the critical load and the related buckling mode shape are then compared with the existing models presented in the previous section (see Eqs. (46) and (47)). The beams of these previous studies are made from isotropic fabric. A present isotropic model is derived from the present orthotropic model to assess the discrepancies between the present model and the other ones besides the orthotropy: it is assumed to be made of the geometric mean isotropic (GMI) material associated with the given orthotropic material, which is proposed by Paschero and Hyer [20]. Instead of the five engineering properties $E_l, E_t, \nu_{lt}, \nu_{tl}$ and G_{lt} , the equivalent GMI material will be described through the three material parameters E_{eq}, ν_{eq} and G_{eq} as follows:

$$E_{eq} = \sqrt{E_l E_t}, \quad \nu_{eq} = \sqrt{\nu_{lt} \nu_{tl}}, \quad G_{eq} = \frac{E_{eq}}{2(1 + \nu_{eq})} \quad (48)$$

with

$$E_{eq} > 0, \quad \nu_{eq}^2 < 1 \quad \text{and} \quad G_{eq} > 0 \quad (49)$$

Two nondimensional parameters will be introduced:

$$e_{lt} = \frac{E_l}{E_t}, \quad g_{lt} = \frac{G_{lt}}{G_{eq}} \quad (50)$$

The parameter e_{lt} measures the level of orthotropy between the two principal directions of the fabric, whereas the parameter g_{lt} measures how much the actual shear modulus G_{lt} differs from the shear modulus G of the GMI material. It should be noted that when both e_{lt} and g_{lt} are equal to unity, the orthotropic material becomes isotropic and coincident with the equivalent GMI material.

The beam is subjected to an internal pressure p first. An external load F is applied at the end in the axial direction of the beam. The mechanical properties given in Table 1 are used [21]. Two ranges of inflation pressure are considered in the analyses. For each pressure the critical loads are calculated to examine the effect of the pressure on the beam behavior. The objective is to validate the present model in case of isotropic material and to point out the discrepancy when adopting an orthotropic behavior and Timoshenko's kinematic in the constitutive equations.

3.1. Simply supported inflatable beam under compressive concentrated load

The first example deals with a simply supported inflatable beam subjected to a compressive concentrated load as shown in

Table 1
Data set for inflatable beam.

Natural thickness, t_ϕ (m)	125×10^{-6}	
Correction shear coefficient, k_y	0.5	
Natural radius, R_ϕ (m)	0.14	
Natural length, l_ϕ (m)	3	
Isotropic fabric's mechanical properties:		
Young modulus, E (MPa)	393.13	
Poisson ratio, ν	0.08	
Orthotropic fabric's mechanical properties:		
	Material 1	Material 2
Young modulus in warp direction, E_l (MPa)	393.13	3940
Young modulus in weft direction, E_t (MPa)	451.59	2920
In-plane shear modulus, G_{lt} (MPa)	103	1118
Poisson ratio, ν_{lt}	0.07	0.23
Poisson ratio, ν_{tl}	0.08	0.17
Internal pressures, p (kPa):		
Low	25	50
High	100	200



Fig. 5. Cantilever inflatable beam.



Fig. 6. Simply supported inflatable beam.



Fig. 7. Clamped-clamped inflatable beam under a compressive axial load.

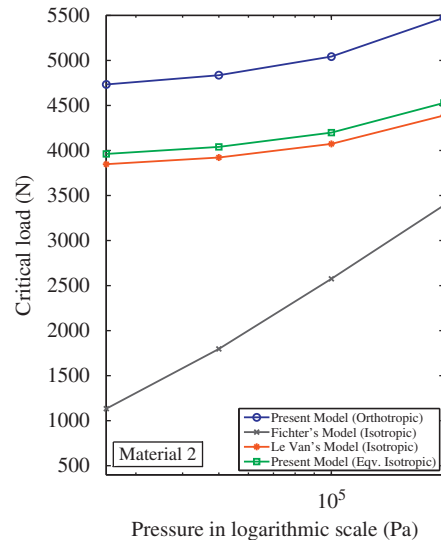
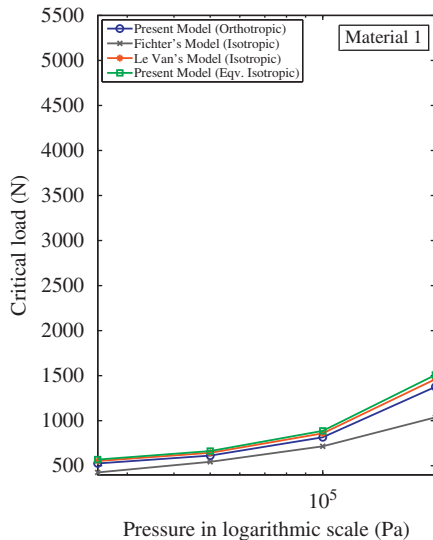


Fig. 8. Critical loads for a simply supported inflatable beam under a compressive concentrated load in the case of materials 1 and 2.

Fig. 6. The boundary conditions corresponding to this case give

$$\begin{cases} v(0) = v(l_0) = 0 \\ \theta_z^{(1)}(0) = \theta_z^{(1)}(l_0) = 0 \end{cases} \quad (51)$$

The boundary conditions and Eq. (42) lead to

$$\begin{cases} \theta_z(X) = C_2 \cos(\Omega X) \\ v(X) = \frac{F_p + C_s^0}{F_p - F + C_s^0} \frac{C_2}{\Omega} \sin(\Omega X) \end{cases} \quad (52)$$

The expression of $v(X)$ corresponds to the buckling mode shapes. These buckling modes are functions of the geometry and the material properties of the membrane.

Using the boundary conditions (51) and the rotation expression given by (52), the quantity Ω can be written as

$$\Omega_n = \frac{n\pi}{l_0} \quad (53)$$

where n is a positive integer which determines the buckling modes. The fundamental buckling mode is obtained for n equal to 1.

This case was studied by Fichter [4] for the inflated circular membranes with an isotropic material. In his expression, Fichter showed the relationship between the bending stiffness and the shear stiffness which includes a shear stiffness component provided by the internal pressure which increases the shear stiffness of an isotropic inflated beam.

In the case of an orthotropic fabric, the results are similar to the ones with an isotropic material except the difference in the critical loads expression due to the level of orthotropy of the material. Fig. 8 shows the critical loads of four inflated beam models at several levels of inflation pressure. In comparison to Fichter's model (relation (46)), the differences are large with 25.13% and 19.01% for the present equivalent isotropic and orthotropic model, respectively, at 25 kPa. These differences are up to 31.26% and 24.66% at 200 kPa. In comparison to Le van's model, the results are in a good agreement with less than 5% for the present equivalent isotropic model and up to -6.21% for the present orthotropic model. These results clearly show that the internal pressure and the fabric characteristics play a key role in the critical loads. The fabric characteristics include the mechanical properties and the level of orthotropy e_{lt} of the fabric, in which the first one governs the value of the critical load while the second one causes the discrepancy between the orthotropic and isotropic models. The inflation pressure only plays a dominant role

when the fabric mechanical properties are poor. As shown in Fig. 8, for material 1, the critical loads of the models are rather equivalent at low pressures, but for higher pressures, the variations become significant between the models. In this case of material, the parameter e_{lt} is less than 1 ($e_{lt} = 0.87$). Thus, the discrepancies between the orthotropic and isotropic models are small. And the critical loads obtained for the present orthotropic model are always below the ones obtained for the equivalent GMI model.

For material 2 (higher moduli and level of orthotropy), the discrepancy between the equivalent GMI and Le van's models is quite small (less than 3%). Except for Fichter's model, there is a large discrepancy between the orthotropic model and two remaining isotropic model. In comparison to Le van's model, the differences are 18.69% and 19.82% at 25 kPa and 200 kPa, respectively. The level of orthotropy in this case of material is high and greater than 1 ($e_{lt} = 1.35$). Consequently, the critical loads of the present orthotropic model are totally over those of the equivalent GMI model. One also note that the inflation pressure does not greatly influence the critical force in that case.

Note that the differences between Fichter's model in comparison to the remaining models in both cases of material, low and high moduli, are always poor. This is because the rotations around the principal axes of inertia of the beam are small and can be neglected. So the shear stiffness does not include the correction shear coefficient in Fichter's expression.

The influence of the fabric mechanical properties and the inflation pressure are also expressed on the fundamental buckling modes (FBM) obtained for the models (Figs. 9 and 10).

One can note also that there is a noticeable discrepancy in the FBM between the present and the reference models at low internal pressure. The present and the reference models become equivalent at the high pressure of 200 kPa (Fig. 9). In the case of material 2, the variations between the present orthotropic model and the isotropic models are almost constant with the increase of the internal pressure except for Fichter's model (Fig. 10). The influence of the orthotropic character is not obvious with a high mechanical properties fabric.

3.2. Cantilever inflatable beam under compressive axial load at the free end

Consider the cantilever beam, shown in Fig. 5, subjected to an internal pressure p and acted upon by a compressive force F at its free-end (Fig. 11).

Together with the displacement boundary condition, boundary conditions (35b) and (35e) give the following relations:

$$\begin{cases} v(0) = \theta_z(0) = 0 \\ v^{(1)}(l_0) = \frac{F_p + C_s^0}{F_p - F + C_s^0} \theta_z(l_0) \\ \theta_z^{(1)}(l_0) = 0 \end{cases} \quad (54)$$

From (54), one obtains the following expressions for the rotation and the deflection:

$$\begin{cases} \theta_z(X) = C_1 \sin(\Omega X) \\ v(X) = \frac{F_p + C_s^0}{F_p - F + C_s^0} \frac{C_1}{\Omega} [1 - \cos(\Omega X)] \end{cases} \quad (55)$$

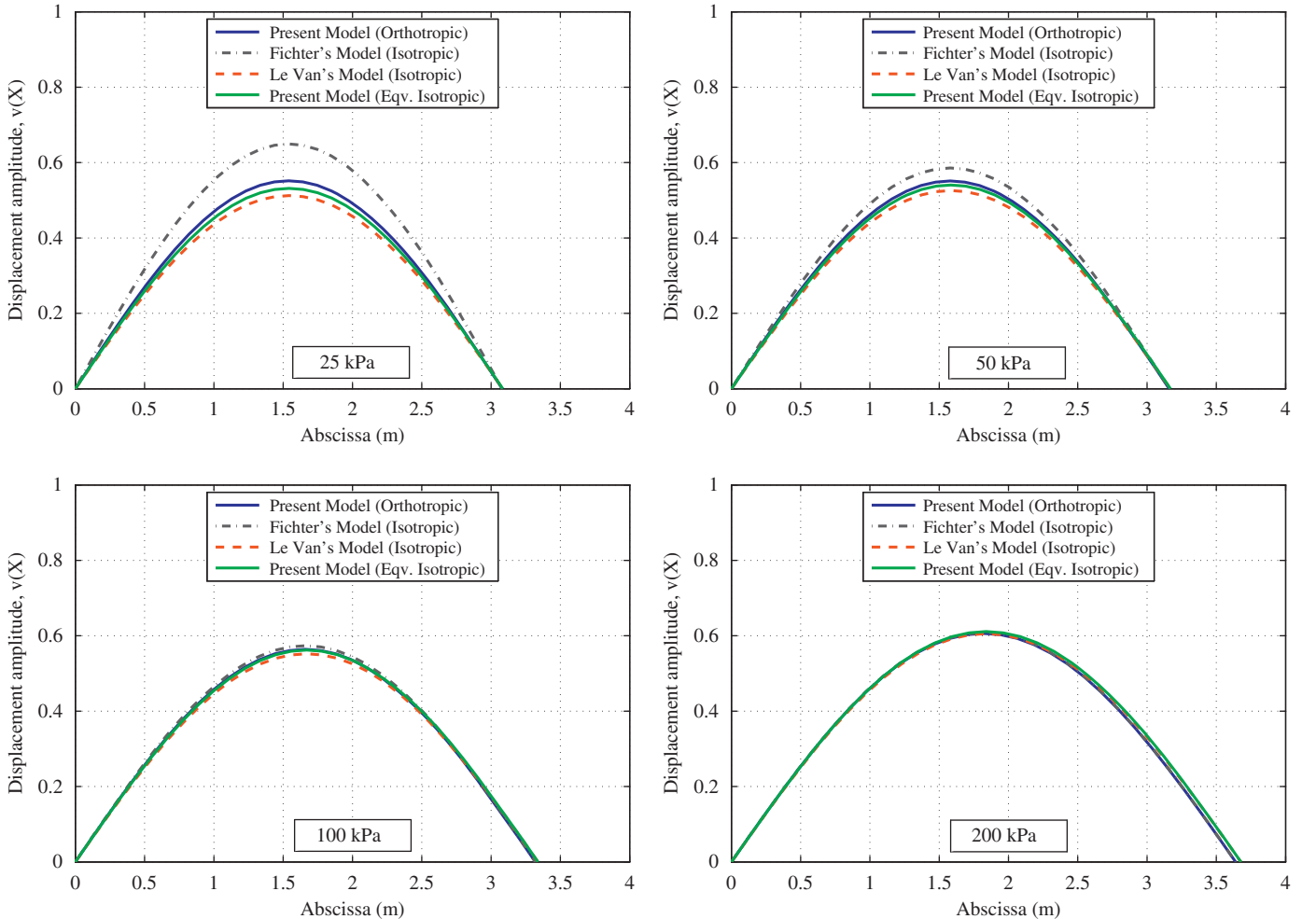


Fig. 9. Fundamental buckling modes on a simply supported inflatable beam under a compressive concentrated load in the case of material 1.

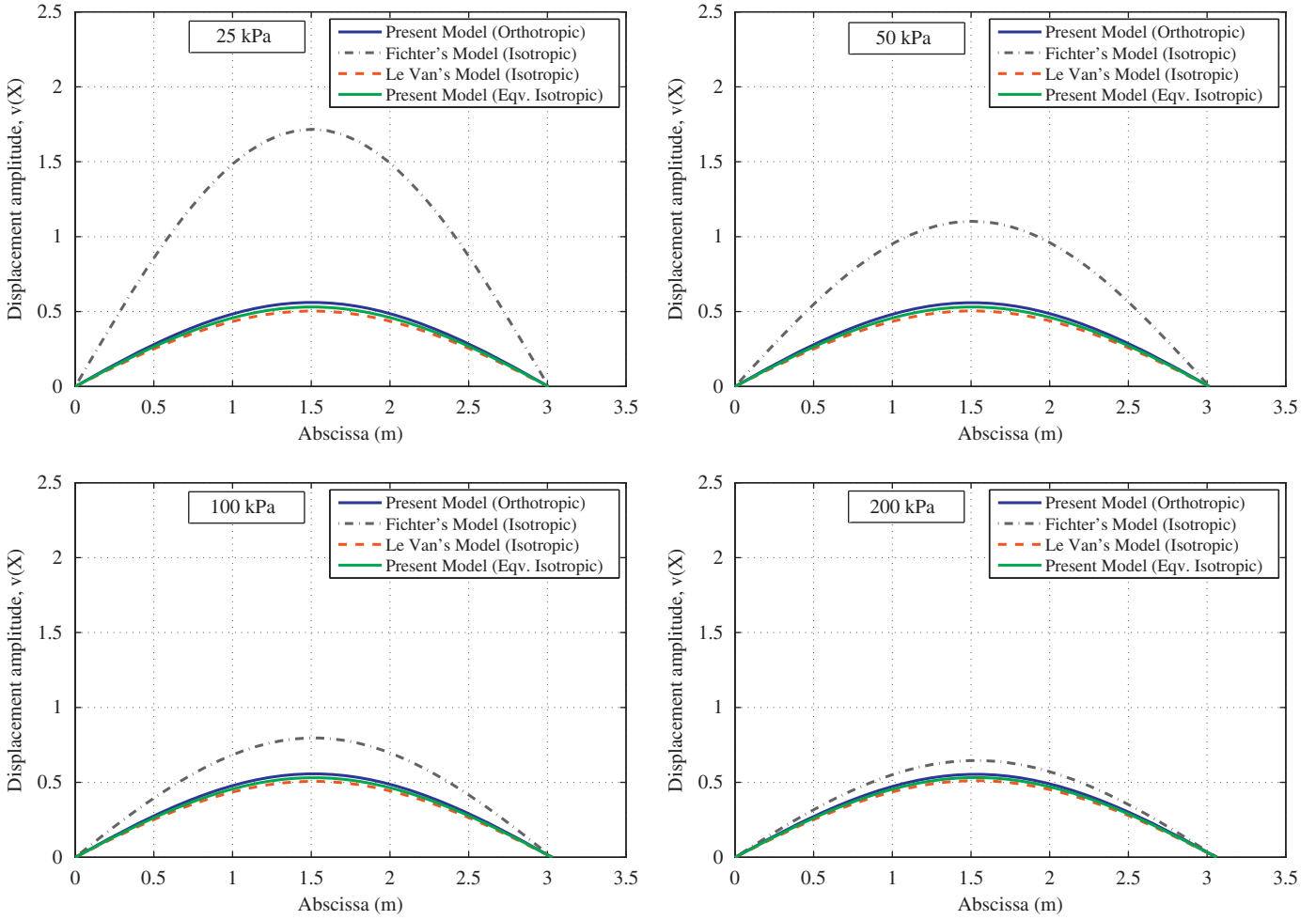


Fig. 10. Fundamental buckling modes on a simply supported inflatable beam under a compressive concentrated load in the case of material 2.

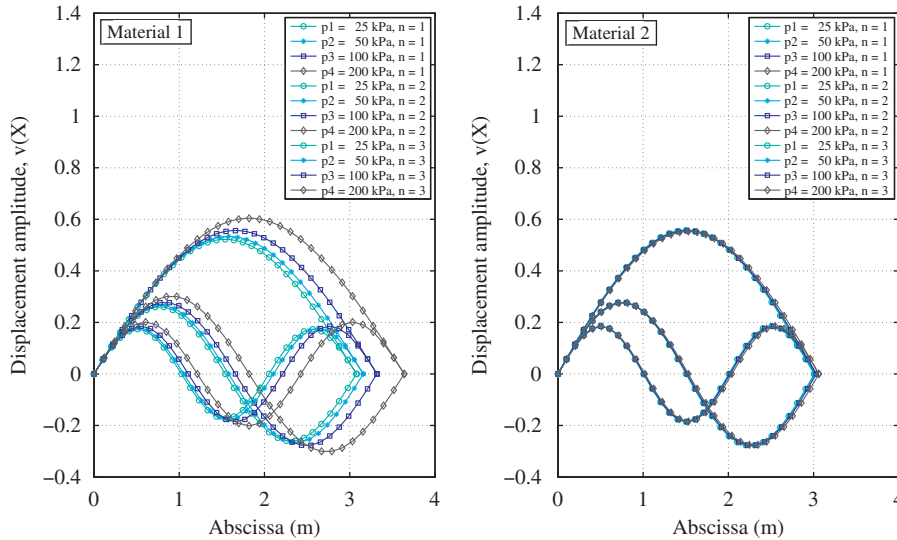


Fig. 11. First three buckling modes on a simply supported HOWF inflatable beam under compressive concentrated load.

Moreover, thanks to the boundary conditions (54), the quantity Ω can be written as

$$\Omega = (2n+1) \frac{\pi}{2l_0} \quad (56)$$

This case has been analyzed by Le van and Wielgosz [5] in the case of isotropic fabric and by the use of the Timoshenko kinematics. Since the beam reference dimensions depend on the fabric properties and the inflation pressure, the values of the critical load and the buckling mode shapes obtained for the four models can be quite different as

shown in Figs. 12–15. Table 1 is still used for the beam properties and the beam dimensions. The differences between the critical load values in the case of clamped-free ends are shown in Table 2.

In the case of material 1, the results are rather similar at low pressure. But for higher pressure over 100 kPa, the results evolve with a small difference in the shear stiffness due to the orthotropic

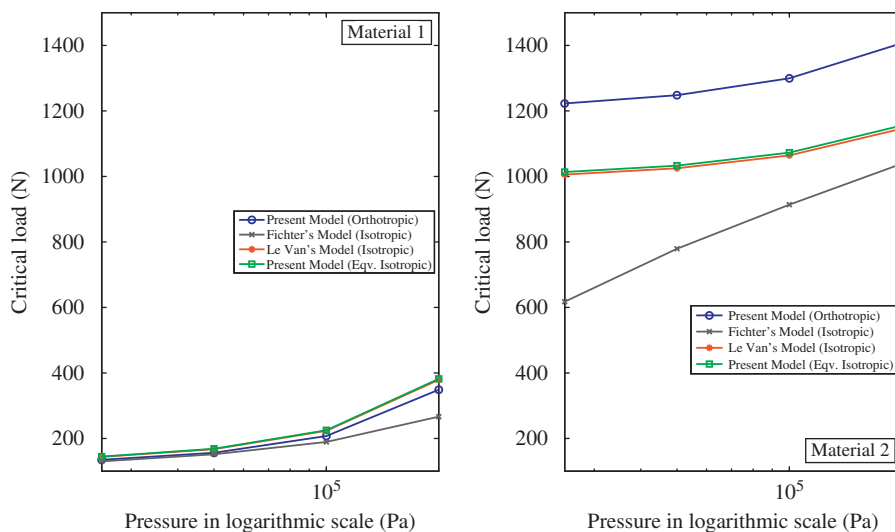


Fig. 12. Critical loads for a cantilever inflatable beam under a compressive concentrated load in the case of materials 1 and 2.

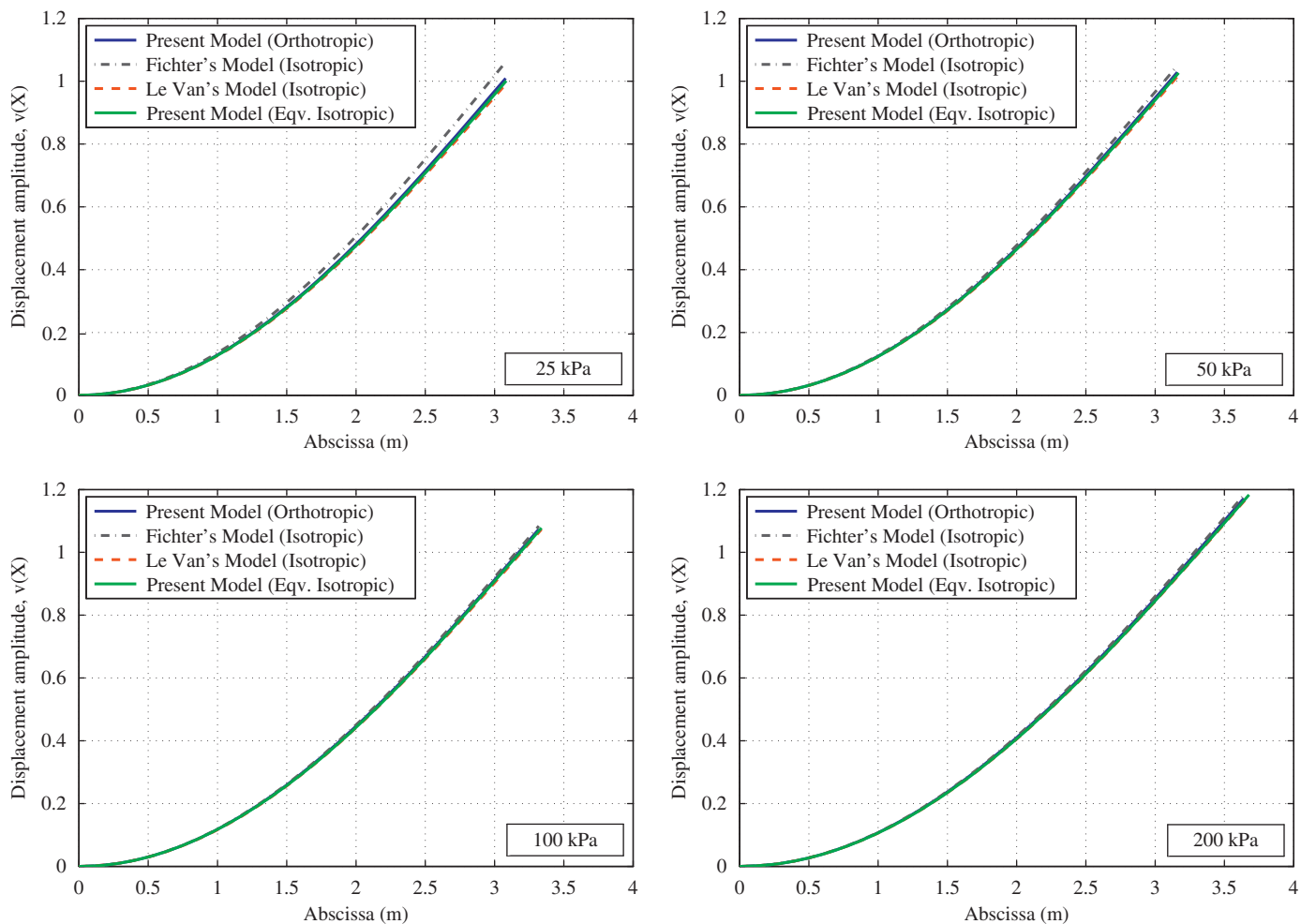


Fig. 13. Fundamental buckling modes on a cantilever inflatable beam under a compressive concentrated load in the case of material 1.

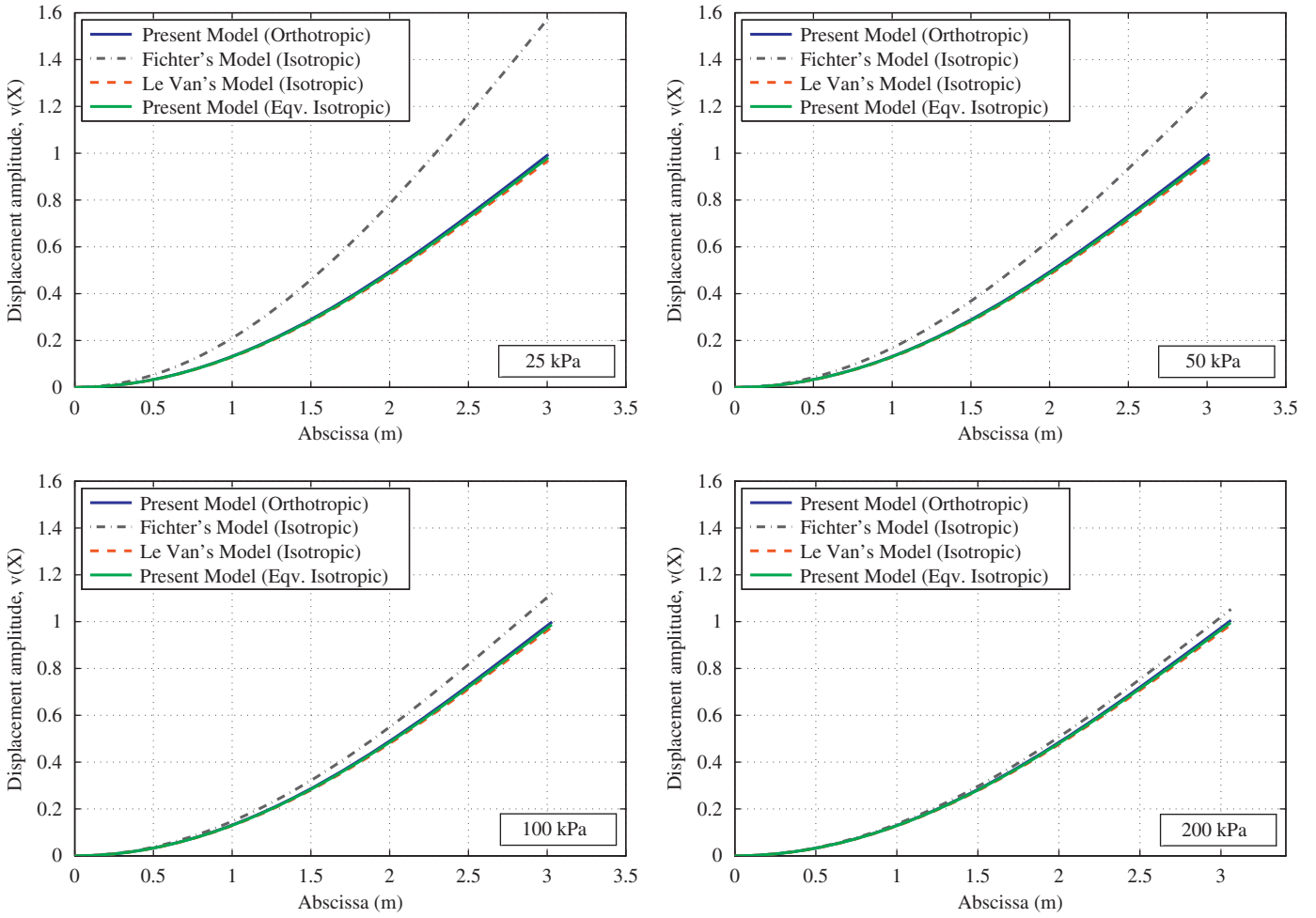


Fig. 14. Fundamental buckling modes on a cantilever inflatable beam under a compressive concentrated load in the case of material 2.

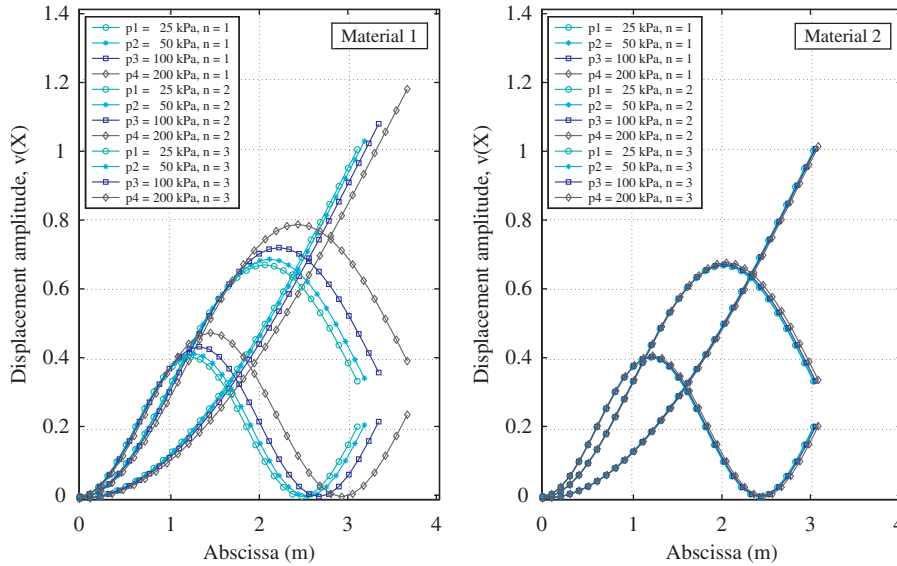


Fig. 15. First three buckling modes on a cantilever inflatable beam under a compressive concentrated load.

character. The effect of the level of orthotropy shows clearly in the case of material 2.

It should be noted that, there is no noticeable difference between the present equivalent isotropic model and Le van's

model in this load case. In both cases of material, the differences between these two models are about 0.8%. A noticeable discrepancy between the present models and Fichter's models in both cases of material is also shown. The results

Table 2
Critical loads of inflatable beam models with various boundary conditions.

Load case	Material	Pressure (kPa)	Critical load $\times 10^2$ (N)				Difference (%)		
			Present		Fichter (Isotropic)	Le Van (Isotropic)	(1) and (3)	(1) and (4)	(2) and (4)
			(Orthotropic) (1)	(Isotropic) (2)	(3)	(4)			
Simply supported	1	25	5.255	5.684	4.256	5.524	19.01	-5.12	2.83
		50	6.125	6.630	5.432	6.435	11.32	-5.07	2.95
		100	8.159	8.598	7.155	8.598	12.31	-5.39	3.05
		200	13.757	15.078	10.365	14.612	24.66	-6.21	3.09
	2	25	47.329	39.619	11.339	38.481	76.04	18.69	2.87
		50	48.352	40.396	17.965	39.221	62.85	18.88	2.91
		100	50.432	41.982	25.754	40.733	48.93	19.23	2.98
		200	54.736	45.279	33.913	43.887	38.04	19.82	3.08
Clamped-free	1	25	1.348	1.448	1.302	1.438	3.41	-6.61	0.75
		50	1.564	1.687	1.515	1.673	3.13	-6.97	0.78
		100	2.075	2.252	1.893	2.233	8.75	-7.64	0.80
		200	3.489	3.822	2.665	3.791	23.63	-8.65	0.81
	2	25	12.228	10.134	6.175	10.056	49.50	17.76	0.77
		50	12.481	10.329	7.792	10.248	37.57	17.89	0.79
		100	12.996	10.726	9.137	10.641	29.69	18.13	0.80
		200	14.067	11.553	10.388	11.459	26.15	18.54	0.82

given by Fichter's model are always poor with high-stiffness material.

For the FBM results, there is no large difference between the models in the case of material 1. The divergence appears in the case of material 2 with Fichter's model. As shown in Figs. 13 and 14, the difference increases along with the beam length and it decreases as the internal pressure increases.

3.3. Clamped-clamped inflatable beam under compressive axial load

The clamped beam is shown in Fig. 7. The boundary conditions to be satisfied are

$$\begin{cases} v(0) = v(l_0) = 0 \\ \theta_z(0) = \theta_z(l_0) = 0 \end{cases} \quad (57)$$

The solution to governing differential (39) is given by (42) and must satisfy the boundary conditions (57). These requirements lead to the linear homogeneous algebraic equations in terms of constants of integration as follows:

$$\begin{bmatrix} 0 & 1 & 0 & 1 \\ \sin(\Omega l_0) & \cos(\Omega l_0) & 1 & 1 \\ \Omega \Gamma^2 l_0 & 0 & 1 & 0 \\ \Omega \Gamma^2 l_0 \cos(\Omega l_0) & -\Omega \Gamma^2 l_0 \sin(\Omega l_0) & 1 & 0 \end{bmatrix} \begin{Bmatrix} B_1 \\ B_2 \\ B_3 \\ B_4 \end{Bmatrix} = \begin{Bmatrix} 0 \\ 0 \\ 0 \\ 0 \end{Bmatrix} \quad (58)$$

For non-trivial solution, the determinant of the systems must vanish. This leads to the following characteristic equation:

$$2[\cos(\Omega l_0) - 1] + \Omega \Gamma^2 l_0 \sin(\Omega l_0) = 0 \quad (59)$$

Note that Ω and Γ are linked together and depend on the axial load. In that case no analytical solution may be derived.

4. Influence of the slenderness ratio on the critical load of an inflatable beam

The following is a discussion of the influence of the beam slenderness ratio on the critical load through the inflation pressure and the material properties. In this section, the buckling of a cantilever inflatable beam is examined in order to address the

evolution of the critical loads as a function of the slenderness ratio.

The slenderness ratio λ has been defined in Section 2: it depends on coefficient μ which is equal to 2 for a cantilever beam. The beam length varies in the range of 0.5–3 m while keeping constant its radius to vary the slenderness ratio. Both materials described in Table 1 are considered; the radius of the beam is given in Table 1. In each case of the material, the internal pressures of 25 kPa and 200 kPa, which correspond to a low and high pressure, are considered in the analyses. The analytical critical load an inflatable beam based on the equations derived by Fichter [4] and Le van and Wielgosz [5] are also included.

As shown in Figs. 16 and 17, the present models agree very well with the models in the literature for large values of λ . As expected, for lower slenderness ratio, Fichter's model overpredicts the critical load: that is most pronounced at the lower inflation pressure.

One also notes that there is a substantial difference between Le van's isotropic model and the present equivalent isotropic model at lower value of λ . This comes from the difference in the way of the establishment of the constitutive equations and the mechanical properties between the models: $E = E_I$ for the isotropic model and E_{eq} (see (48)) for the present equivalent isotropic model.

The results highlight the importance of including the shear deformations and the pressure effects. Obviously, an inflatable beam with higher inflation pressures is clearly more stable whatever the boundary conditions.

5. Wrinkling load for an inflatable beam under a compressive concentrated load

When a membrane is subjected to a compression load in one principal direction and to a tension load in the other direction, it buckles and many narrow wrinkles appear. It is difficult to account for the wrinkling phenomena which cannot be predicted by the standard membrane theories. A membrane wrinkling theory should not allow any negative stress to appear. When a negative (compressive) stress is about to appear the membrane will wrinkle and the negative stress should vanish. Concerning the inflatable cylindrical

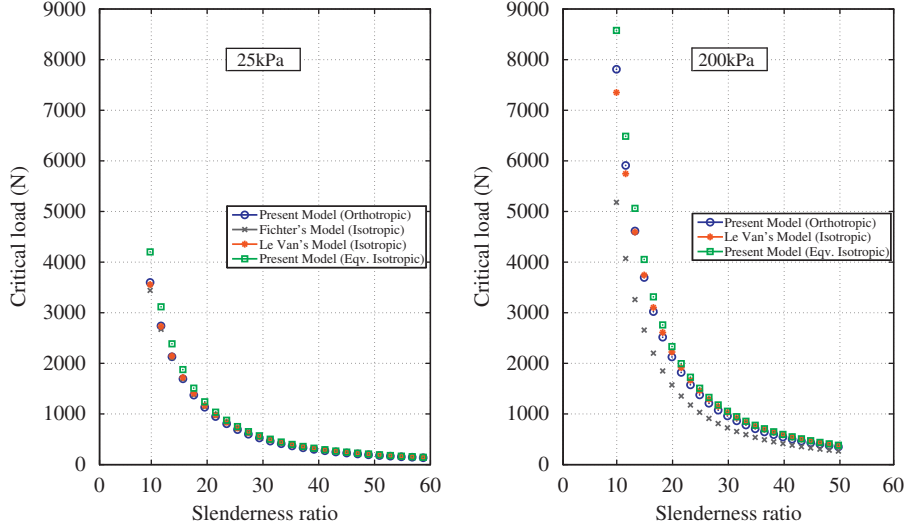


Fig. 16. Critical load versus the slenderness ratio of a cantilever inflatable beam under compressive concentrated load in the case of material 1.

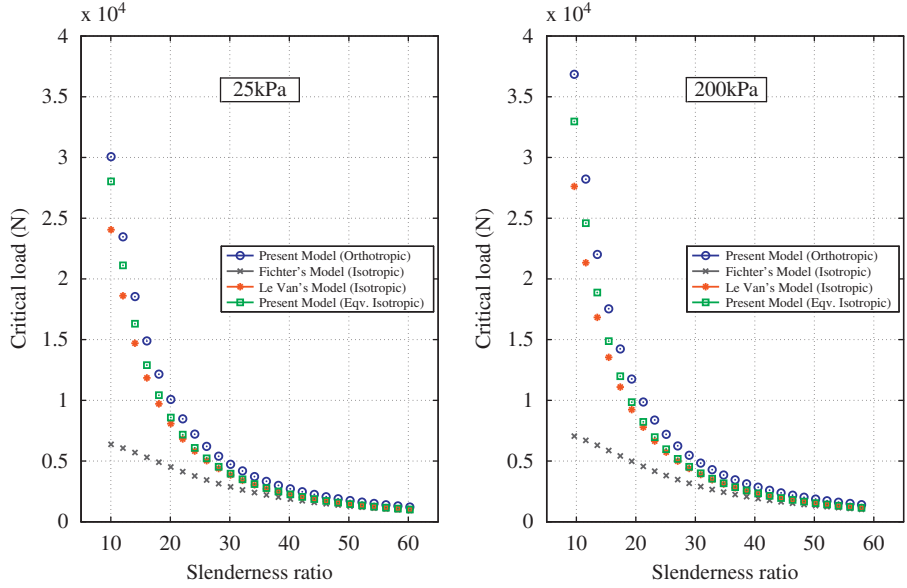


Fig. 17. Critical load versus the slenderness ratio of a cantilever inflatable beam under compressive concentrated load in the case of material 2.

beams, many studies have dealt with the wrinkling phenomenon [1–3,5,7,9,13,22,23]. The theoretical model developed in this paper supposes that no wrinkle occurs. However the fabric used for the inflatable beams is a membrane. So, there exists a load (the wrinkling load) from which the first wrinkles appear and the proposed model is no longer valid if it happens before the buckling. This load depends on the inflation pressure, the geometrical parameters and the material properties. To determine the wrinkling load of thin-walled structures, two possible criteria can be used: the non-negative principal stresses or the non-negative principal strains. In this work, the stress criterion was adopted. From (9) the principal stress is obtained:

$$S1 \approx \sigma_{xx} = \frac{N^0}{A_0} \quad (60)$$

In general, for inflatable structures, the inflation stiffness is a major factor responsible for buckling and wrinkling. Once the stress in the axial fibers becomes zero, wrinkling occurs resulting in a significant loss of inflation stiffness. The wrinkling criterion

used is finally given by

$$S1 > 0 \quad (61)$$

The expression for the principal stress in this case is then given by (60), and as mentioned in Section 2.4, the initial force is $N^0(X) = F_p - F$. From (61), the validity condition of the solution can be written as

$$N^0 = F_p - F > 0 \quad (62)$$

At the limit point, the axial load F becomes the wrinkling load F_w which is then obtained:

$$F_w = F_p = p\pi R_0^2 \quad (63)$$

The wrinkling load in this case is a function of the internal pressure, the geometry of the beam, and the mechanical properties of the fabric through R_0 (see Eq. (3)). Since the axial load due to the inflation represents the stiffness of the inflatable beam, the wrinkling load is herein defined as the upper bound of the axial load. Beyond this bound, the inflated beam will collapse whatever

the fabric stiffness. Following (43), the critical load is proportional to the inflation pressure and the mechanical properties of the fabric: the beams made in a high mechanical property fabric will have a high critical load that may exceed the wrinkling load which weakly depends on the mechanical properties of the beam. In this case, the critical load is the wrinkling load.

6. Conclusion

An analytical approach to approximate the critical load for an HOWF 3D Timoshenko beam was proposed in this paper. Regarding the buckling behavior, the proposed inflatable beam model showed a good agreement with the previous models in the literature.

The total Lagrangian form of the virtual work principle and Timoshenko kinematics were used to derive the beam's governing equations. By solving these linearized equations, an analytical expression of the critical buckling load was obtained.

A parametric study was performed to show the discrepancy on the critical load due to the orthotropic character between the present model and the isotropic models in the literature. One can see that both the inflation pressure and the fabric characteristics govern the critical load. The fabric characteristics include the mechanical properties and the level of orthotropy of the fabric, in which the first one governs the value of the critical load while the second one causes the discrepancy between the orthotropic and isotropic models. The results showed that the analytical solution obtained from Fichter's equations overpredict the critical load as well.

By taking into account the orthotropic character in the present model, the study pointed out that only the mechanical properties E_t and G_{lt} intervene explicitly in the solution of critical load through C_{11} and C_{66} while E_t intervenes implicitly through the reference dimensions of the beam. Only the level of orthotropy of the fabric causes noticeable discrepancies in the buckling behavior of the inflatable beam. This comes from the inequality of the mechanical properties in the yarn directions. The differences between the models studied also come from the way of the establishment of the constitutive equations. In Le van's model, the material is assumed to be hyperelastic isotropic and obeying the Saint Venant-Kirchhoff law in which only S_{XX} and S_{YY} are taken into account. The Young modulus E is also used directly in the Hookean stress-strain relationship. In the present model, we take into account all components of the second Piola-Kirchhoff tensor. The elasticity tensor with the tensor components described the mechanical properties of the orthotropic material is used instead of the Young modulus E .

The inflation pressure has a significant influence on the buckling behavior of the present model. It was also noted that for a sufficient internal pressure (the critical solution to be meaningful), the prediction of the stability of inflatable structures is more accurate and can be simplified with a high-stiffness fabric.

Regarding the limit of the validity of the theory, the wrinkling load is taken as a reference upper bound for the axial load of an inflatable cantilever beam. So, the critical loads found in Section 3 must not be exceeded the wrinkling load for the buckling solution to be meaningful.

This work provided an analytical expression for the critical load of an HOWF inflatable beam. Then, by using this expression, it is possible to get round the buckling analysis using a finite element method. A linear eigenbuckling and a nonlinear buckling analysis will be attempted on the HOWF beam in a further research. The computation of the critical loads and the use of an incremental iterative strategy for approaching the limit points and the bifurcation points will be performed.

Acknowledgments

This work was supported by Laboratory Design of Structures (Laboratory DDS of GMP, IUT Lyon 1, University of Claude Bernard) and the consultant Mr. Robert Dartois.

Appendix A

The expressions of the axial force, the shear forces and the quantities Q_i ($i = 1, \dots, 10$) depending on the initial geometry of the cross-section, are given here. These quantities are presented in (19) and (20):

$$N = \int_{A_0} S_{XX} dA = N^0 + \left\{ C_{11} \left[u_{,X} + \frac{1}{2} (u_{,X}^2 + v_{,X}^2 + w_{,X}^2) \right] + \frac{1}{4} C_{12} (\theta_Y^2 + \theta_Z^2) \right\} A_0 + \frac{1}{2} C_{11} I_0 (\theta_{Y,X}^2 + \theta_{Z,X}^2)$$

$$T_y = \int_{A_0} S_{XY} dA = \frac{1}{2} k_y A_0 C_{66} [v_{,X} - \theta_Z (1 + u_{,X})]$$

$$T_z = \int_{A_0} S_{XZ} dA = \frac{1}{2} k_z A_0 C_{66} [w_{,X} + \theta_Y (1 + u_{,X})]$$

$$M_y = \int_{A_0} Z S_{XX} dA = (1 + u_{,X}) C_{11} \theta_{Y,X} I_0$$

$$M_z = - \int_{A_0} Y S_{XX} dA = (1 + u_{,X}) C_{11} \theta_{Z,X} I_0$$

and

$$Q_1 = - \int_{A_0} Y Z S_{XX} dA = \frac{1}{4} I_0 (C_{11} R_0^2 \theta_{Z,X} \theta_{Y,X} - C_{12} \theta_Z \theta_Y)$$

$$Q_2 = \int_{A_0} Z^2 S_{XX} dA = \left\{ \frac{N^0}{A_0} + C_{11} \left[u_{,X} + \frac{1}{2} (u_{,X}^2 + v_{,X}^2 + w_{,X}^2) + \frac{1}{8} R_0^2 (3\theta_{Y,X}^2 + \theta_{Z,X}^2) \right] + \frac{1}{8} C_{12} (3\theta_Z^2 + \theta_Y^2) \right\} I_0$$

$$Q_3 = - \int_{A_0} Z S_{XY} dA = \frac{1}{4} C_{66} I_0 (3\theta_Z \theta_{Y,X} - \theta_Y \theta_{Z,X})$$

$$Q_4 = \int_{A_0} Z S_{XZ} dA = \frac{1}{4} C_{66} I_0 (\theta_Y \theta_{Y,X} - \theta_Z \theta_{Z,X})$$

$$Q_5 = \int_{A_0} Y^2 S_{XX} dA = \left\{ \frac{N^0}{A_0} + C_{11} \left[u_{,X} + \frac{1}{2} (u_{,X}^2 + v_{,X}^2 + w_{,X}^2) + \frac{1}{8} R_0^2 (\theta_{Y,X}^2 + 3\theta_{Z,X}^2) \right] + \frac{1}{8} C_{12} (\theta_Z^2 + 3\theta_Y^2) \right\} I_0$$

$$Q_6 = \int_{A_0} Y S_{XY} dA = \frac{1}{4} C_{66} I_0 (\theta_Z \theta_{Z,X} - \theta_Y \theta_{Y,X})$$

$$Q_7 = - \int_{A_0} Y S_{XZ} dA = \frac{1}{4} C_{66} I_0 (3\theta_{Z,X} \theta_Y - \theta_Z \theta_{Y,X})$$

$$Q_8 = \int_{A_0} S_{YY} dA = N^0 + \frac{1}{2} A_0 \left\{ C_{12} \left[u_{,X} + \frac{1}{2} (u_{,X}^2 + v_{,X}^2 + w_{,X}^2) \right] + \frac{1}{8} C_{22} (3\theta_Z^2 + \theta_Y^2) \right\} + \frac{1}{8} C_{12} I_0 (3\theta_{Y,X}^2 + \theta_{Z,X}^2)$$

$$Q_9 = \int_{A_0} S_{ZZ} dA = N^0 + \frac{1}{2} A_0 \left\{ C_{12} \left[u_{,X} + \frac{1}{2} (u_{,X}^2 + v_{,X}^2 + w_{,X}^2) \right] + \frac{1}{8} C_{22} (3\theta_Y^2 + \theta_Z^2) \right\} + \frac{1}{8} C_{12} I_0 (3\theta_{Z,X}^2 + \theta_{Y,X}^2)$$

$$Q_{10} = - \int_{A_0} S_{YZ} dA = \frac{1}{8} C_{22} A_0 \theta_Y \theta_Z - \frac{1}{4} C_{12} I_0 \theta_{Y,X} \theta_{Z,X}$$

The force terms used in the expression of virtual work (21):

$$A_1(X) = \begin{Bmatrix} N \\ M_y \\ M_z \\ -T_y \\ T_z \end{Bmatrix}^T \times \begin{Bmatrix} 1+u_x \\ \theta_{Y,X} \\ \theta_{Z,X} \\ \theta_Z \\ \theta_Y \end{Bmatrix}, \quad B_1(X) = \begin{Bmatrix} N \\ T_y \end{Bmatrix}^T \times \begin{Bmatrix} v_x \\ 1 \end{Bmatrix}$$

$$C_1(X) = \begin{Bmatrix} N \\ T_z \end{Bmatrix}^T \times \begin{Bmatrix} w_x \\ 1 \end{Bmatrix}, \quad D_1(X) = \begin{Bmatrix} T_z \\ Q_4 \\ Q_7 \\ Q_9 \\ Q_{10} \end{Bmatrix}^T \times \begin{Bmatrix} 1+u_x \\ \theta_{Y,X} \\ \theta_{Z,X} \\ \theta_Y \\ \theta_Z \end{Bmatrix}$$

$$E_1(X) = \begin{Bmatrix} M_y \\ Q_1 \\ Q_2 \\ Q_3 \\ Q_4 \end{Bmatrix}^T \times \begin{Bmatrix} 1+u_x \\ \theta_{Z,X} \\ \theta_{Y,X} \\ \theta_Z \\ \theta_Y \end{Bmatrix}, \quad F_1(X) = \begin{Bmatrix} -T_y \\ Q_3 \\ Q_6 \\ Q_8 \\ Q_{10} \end{Bmatrix}^T \times \begin{Bmatrix} 1+u_x \\ \theta_{Y,X} \\ \theta_{Z,X} \\ \theta_Z \\ \theta_Y \end{Bmatrix}$$

$$H_1(X) = \begin{Bmatrix} M_z \\ Q_5 \\ Q_1 \\ Q_6 \\ Q_7 \end{Bmatrix}^T \times \begin{Bmatrix} 1+u_x \\ \theta_{Z,X} \\ \theta_{Y,X} \\ \theta_Z \\ \theta_Y \end{Bmatrix}$$

References

- [1] Comer R, Levy S. Deflections of an inflated circular cylindrical cantilever beam. *AIAA* 1963;1(7):1652–5.
- [2] Main J, Peterson S, Strauss A. Load–deflection behavior of space-based inflatable fabric beams. *Journal of Aerospace Engineering* 1994;7(2):225–38.
- [3] Main J, Peterson S, Strauss A. Beam-type bending of space-based membrane structures. *Journal of Aerospace Engineering* 1995;8(2):120–5.

- [4] Fichter, W. A theory for inflated thin wall cylindrical beams. Technical Report, NASA Technical Note, NASA TND-3466; 1966.
- [5] Le van A, Wielgosz C. Bending and buckling of inflatable beams: some new theoretical results. *Thin-Walled Structures* 2005;43(8):1166–87.
- [6] Davids WG, Zhang H. Beam finite element for nonlinear analysis of pressurized fabric beam-columns. *Engineering Structures* 2008;30(7):1969–80.
- [7] Apedo K, Ronel S, Jacquelin E, Massenzio M, Bennani A. Theoretical analysis of inflatable beams made from orthotropic fabric. *Thin-Walled Structures* 2009;47(12):1507–22.
- [8] Apedo K, Ronel S, Jacquelin E, Bennani A, Massenzio M. Nonlinear finite element analysis of inflatable beams made from orthotropic woven fabric. *International Journal of Solids and Structures* 2010;47(16):2017–33.
- [9] Le van A, Wielgosz C. Finite element formulation for inflatable beams. *Thin-Walled Structures* 2007;45(2):221–36.
- [10] Haughton D, McKay B. Wrinkling of inflated elastic cylindrical membranes under flexure. *International Journal of Engineering Science* 1996;34(13):1531–50.
- [11] Molloy S. Finite element analysis of a pair of leaning pressurized arch-shells under snow and wind loads. PhD thesis, MS thesis. Blacksburg, VA: Virginia Polytechnic Institute and State University; 1998.
- [12] Plaut RH, Goh JK, Kigudde M, Hammerand DC. Shell analysis of an inflatable arch subjected to snow and wind loading. *International Journal of Solids and Structures* 2000;37(31):4275–88.
- [13] Diaby A, van AL, Wielgosz C. Buckling and wrinkling of prestressed membranes. *Finite Elements in Analysis and Design* 2006;42(11):992–1001.
- [14] NASA, Buckling of thin-walled circular cylinders. Technical Report, NASA Space vehicle design criteria. NASA SP-8007; 1965.
- [15] Batoz J, Dhatt G. Modélisation des structures par éléments finis. Paris: Hermès; 1990.
- [16] Saadé K, Espion B, Warzée G. Flexural torsional buckling of three dimensional thin walled elastic beams. In: 15th ASCE engineering mechanics conference. New York, NY: Columbia University; 2002.
- [17] Apedo KL. Numerical modelling of inflatable structures made of orthotropic technical textiles: application to the frames of inflatable tents. PhD thesis. University of Claude Bernard Lyon 1; 2010.
- [18] Cowper GR. The shear coefficient in Timoshenko's beam theory. *Journal of Applied Mechanics* 1966;33(2):335–40.
- [19] Gambhir ML. Stability analysis and design of structures. Berlin, Heidelberg: Springer-Verlag; 2004.
- [20] Paschero M, Hyer MW. Axial buckling of an orthotropic circular cylinder: application to orthogrid concept. *International Journal of Solids and Structures* 2009;46(10):2151–71. (Special issue in Honor of Professor Liviu Librescu).
- [21] Vysochina K. Comportement des textiles techniques souples dans le domaine des grandes déformations; indentification de la rigidité en cisaillement plan. PhD thesis. Université Claude Bernard Lyon 1; 2005.
- [22] Suhey JD, Kim NH, Niezrecki C. Numerical modeling and design of inflatable structures—application to open-ocean-aquaculture cages. *Aquacultural Engineering* 2005;33(4):285–303.
- [23] Veldman S. Wrinkling prediction of cylindrical and conical inflated cantilever beams under torsion and bending. *Thin-Walled Structures* 2006;44(2):211–5.